Supplemental Online Materials

Methods

Results included in this manuscript come from preprocessing performed using fMRIPrep 1.5.8 (Esteban, Markiewicz, et al. (2018); Esteban, Blair, et al. (2018); RRID:SCR_016216), which is based on Nipype 1.4.1 (Gorgolewski et al. (2011); Gorgolewski et al. (2018); RRID:SCR_002502). The anatomical and functional neuroimaging data preprocessing sections below are based on boilerplate text generated by fMRIPrep.

Anatomical neuroimaging data preprocessing using fmriprep

The T1-weighted (T1w) image was corrected for intensity non-uniformity (INU) with N4BiasFieldCorrection (Tustison et al. 2010), distributed with ANTs 2.2.0 (Avants et al. 2008, RRID:SCR_004757), and used as T1w-reference throughout the workflow. The T1w-reference was then skull-stripped with a Nipype implementation of the antsBrainExtraction.sh workflow (from ANTs), using OASIS30ANTs as target template. Brain tissue segmentation of cerebrospinal fluid (CSF), white-matter (WM) and gray-matter (GM) was performed on the brain-extracted T1w using fast (FSL 5.0.9, RRID:SCR_002823, Zhang, Brady, and Smith 2001). Volume-based spatial normalization to one standard space (MNI152NLin6Asym) was performed through nonlinear registration with antsRegistration (ANTs 2.2.0), using brain-extracted versions of both T1w reference and the T1w template. The following template was selected for spatial normalization: FSL's MNI ICBM 152 non-linear 6th Generation Asymmetric Average Brain Stereotaxic Registration Model [Evans et al. (2012), RRID:SCR_002823; TemplateFlow ID: MNI152NLin6Asym].

Functional neuroimaging data preprocessing using fmriprep

For each BOLD run per subject, the following preprocessing was performed. First, a reference volume and its skull-stripped version were generated using a custom methodology of fMRIPrep. A B0-nonuniformity map (or fieldmap) was estimated based on a phase-difference map calculated with a dual-echo GRE (gradient-recall echo) sequence, processed with a custom workflow of SDCFlows inspired by the epidewarp.fsl script and further improvements in HCP Pipelines (Glasser et al. 2013). The fieldmap was then co-registered to the target EPI (echo-planar imaging) reference run and converted to a displacements field map (amenable to registration tools such as ANTs) with FSL's fugue and other SDCflows tools. Based on the estimated susceptibility distortion, a corrected EPI (echo-planar imaging) reference was calculated for a more accurate coregistration with the anatomical reference. The BOLD reference was then co-registered to the T1w reference using flirt (FSL 5.0.9, Jenkinson and Smith 2001) with the boundary-based registration (Greve and Fischl 2009) cost-function. Co-registration was configured with nine degrees of freedom to account for distortions remaining in the BOLD reference. Head-motion parameters with respect to the BOLD reference (transformation matrices, and six corresponding rotation and translation parameters) are estimated before any spatiotemporal filtering using mcflirt (FSL 5.0.9, Jenkinson et al. 2002). BOLD runs were slice-time corrected using 3dTshift from AFNI 20160207 (Cox and Hyde 1997, RRID:SCR 005927). The BOLD time-series (including slice-timing correction when applied) were resampled onto their original, native space by applying a single, composite transform to correct for head-motion and susceptibility distortions. These resampled BOLD time-series will be referred to as preprocessed BOLD in original space, or just preprocessed BOLD. The BOLD time-series were resampled into standard space, generating a preprocessed BOLD run in ['MNI152NLin6Asym'] space. First, a reference volume and its skull-stripped

version were generated using a custom methodology of fMRIPrep. Automatic removal of motion artifacts using independent component analysis (ICA-AROMA, Pruim et al. 2015) was performed on the preprocessed BOLD on MNI space time-series after removal of non-steady state volumes and spatial smoothing with an isotropic, Gaussian kernel of 6mm FWHM (full-width halfmaximum). Corresponding "non-aggresively" denoised runs were produced after such smoothing. Additionally, the "aggressive" noise-regressors were collected and placed in the corresponding confounds file. Several confounding time-series were calculated based on the preprocessed BOLD: framewise displacement (FD), DVARS and three region-wise global signals. FD and DVARS are calculated for each functional run, both using their implementations in Nipype (following the definitions by Power et al. 2014). The three global signals are extracted within the CSF, the WM, and the whole-brain masks. Additionally, a set of physiological regressors were extracted to allow for component-based noise correction (CompCor, Behzadi et al. 2007). Principal components are estimated after high-pass filtering the preprocessed BOLD time-series (using a discrete cosine filter with 128s cut-off) for the two CompCor variants: temporal (tCompCor) and anatomical (aCompCor). tCompCor components are then calculated from the top 5% variable voxels within a mask covering the subcortical regions. This subcortical mask is obtained by heavily eroding the brain mask, which ensures it does not include cortical GM regions. For aCompCor, components are calculated within the intersection of the aforementioned mask and the union of CSF and WM masks calculated in T1w space, after their projection to the native space of each functional run (using the inverse BOLD-to-T1w transformation). Components are also calculated separately within the WM and CSF masks. For each CompCor decomposition, the k components with the largest singular values are retained, such that the retained components' time series are sufficient to explain 50 percent of variance across the nuisance mask (CSF, WM, combined, or temporal). The remaining components are dropped from consideration. The head-motion estimates calculated in the correction step were also placed within the corresponding confounds file. The confound time series derived from head motion estimates and global signals were expanded with the inclusion of temporal derivatives and quadratic terms for each (Satterthwaite et al. 2013). All resamplings can be performed with a single interpolation step by composing all the pertinent transformations (i.e. head-motion transform matrices, susceptibility distortion correction when available, and coregistrations to anatomical and output spaces). Gridded (volumetric) resamplings were performed using antsApplyTransforms (ANTs), configured with Lanczos interpolation to minimize the smoothing effects of other kernels (Lanczos 1964). Non-gridded (surface) resamplings were performed using mri vol2surf (FreeSurfer). Functional data were then highpass filtered with a cutoff period of 100s.

GLM specification

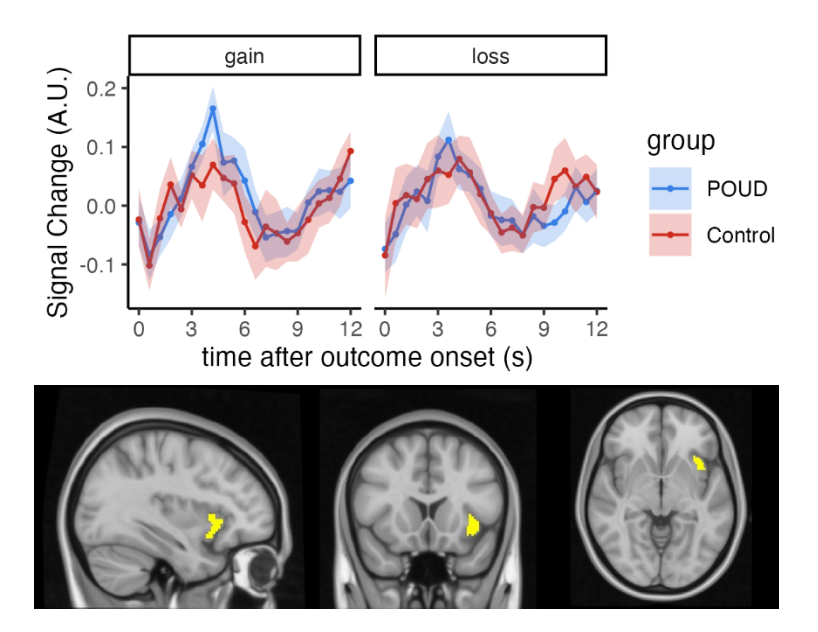
In addition to the task events indicators described in the main text (gain, loss, and no outcome), the first level GLM included 1 regressor indicating onset of the response phase of each trial (duration equal to the trial response time), and 1 regressor indicating missed trials where no response was made during the 2s response window (if any responses were missed). Each of these previously specified regressors was convolved with a standard hemodynamic response function (double gamma function in FSL; Smith et al., 2004) and included in the first level GLM along with its temporal derivative. 24 expanded head motion-related confound regressors (6 rigid body translation and rotation parameters, square of the 6 parameters, temporal derivative of the 6 parameters, and square of the temporal derivative of the 6 parameters) were included in the model. Additionally, outlier volumes were identified and removed by including a regressor for each outlier

volume. Outlier volumes were identified by root-mean-square intensity difference of each volume relative to the next (DVARS in *fsl_motion_outliers*, Jenkinson et al., 2012; Smith et al., 2004) using a boxplot threshold: 75th percentile plus 1.5 times the interquartile range).

Supplementary Results

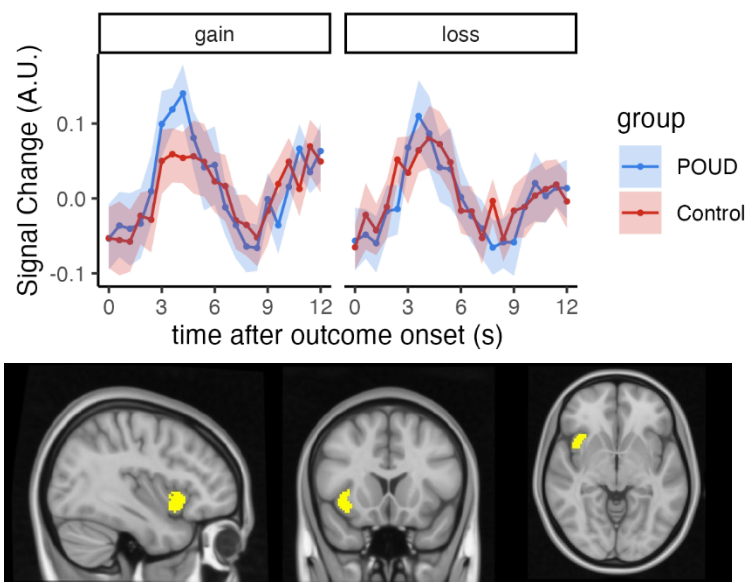
Additional Regions of Interest. Regions of interest were defined from a meta-analysis of neuroimaging studies examining fMRI responses to rewards and punishment (Bartra et al., 2013). 8 additional regions were defined from this meta-analysis (Figure 3A-B in Bartra et al., 2013 identified regions that show consistent representations of reward or punishment value): left ventral striatum, right ventral striatum, left VMPFC, right VMPFC, left anterior insula, right anterior insula, left pre-SMA, right pre-SMA, left amygdala, right amygdala, left posterior cingulate, and right posterior cingulate. A time series plot of fMRI BOLD signal change following monetary gain and loss outcomes is included above an image of each region. Statistics (F-statistic, uncorrected p-value, partial η^2) are below each image to show main effects of group and group by time point interactions from the group (POUD, control) by time point (0-12s) ANOVA conducted on responses to gain and loss in each region (age and sex were included as covariates).

Left anterior insula signal change following gain and loss



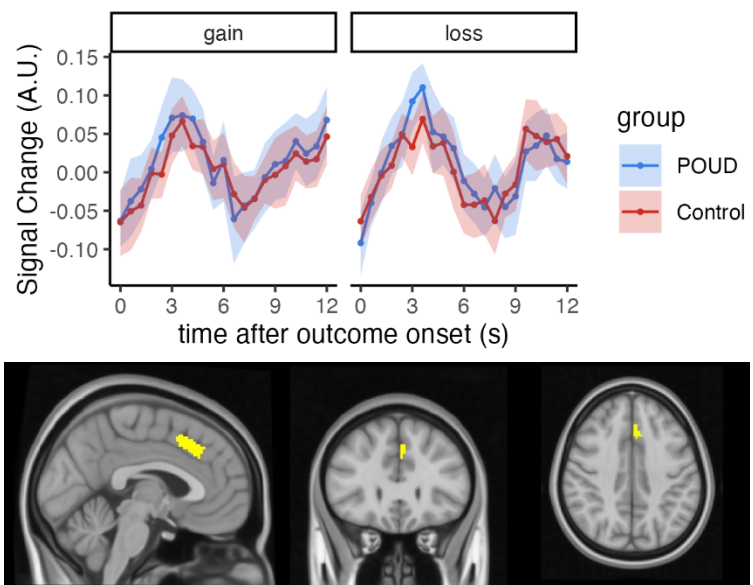
Main effect of group in responses to gain: F(1,40) = 7.181, p = .011, $\eta^2 = 0.015*$ Group by time interaction in responses to gain: F(7.59, 303.43) = 1.953, p = .056, $\eta^2 = 0.043$ Main effect of group in responses to loss: F(1,40) = 0.398, p = .532, $\eta^2 = 0.001$ Group by time interaction in responses to loss: F(6.25, 250.06) = 0.738, p = .625, $\eta^2 = 0.016$

Right anterior insula signal change following gain and loss



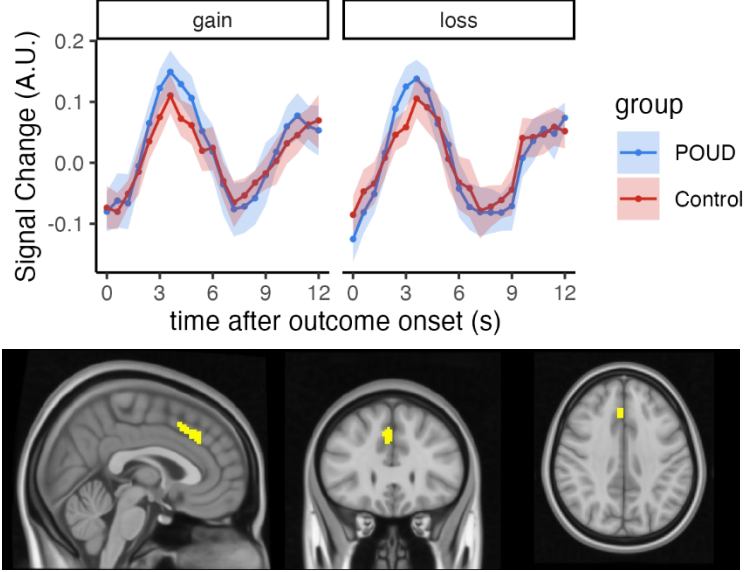
Main effect of group in responses to gain: F(1,40) = 2.284, p = .139, $\eta^2 = 0.007$ Group by time interaction in responses to gain: F(7.42, 296.75) = 1.490, p = .166, $\eta^2 = 0.032$ Main effect of group in responses to loss: F(1,40) = 0.240, p = .627, $\eta^2 = .001$ Group by time interaction in responses to loss: F(12, 480) = 1.339, p = .193, $\eta^2 = .028$

Left pre-SMA signal change following gain and loss



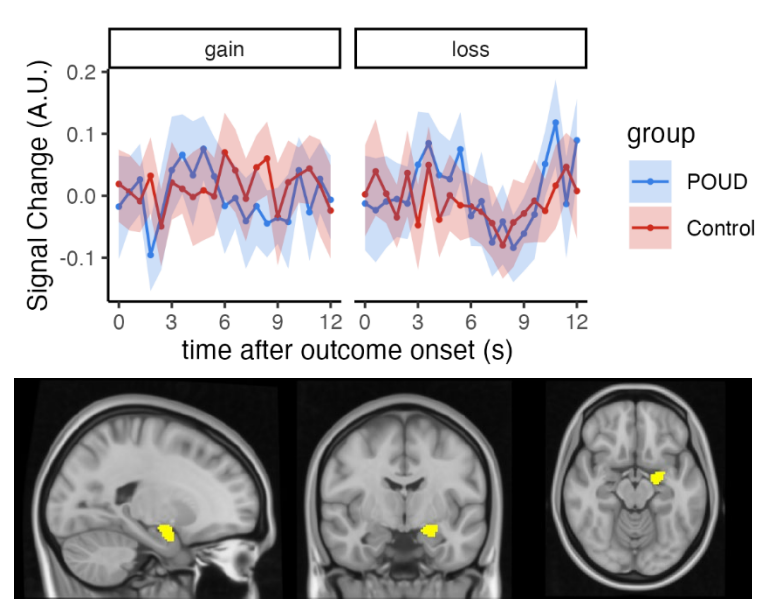
Main effect of group in responses to gain: F(1,40) = 2.284, p = .139, $\eta^2 = 0.007$ Group by time interaction in responses to gain: F(7.42, 296.75) = 1.490, p = .166, $\eta^2 = 0.032$ Main effect of group in responses to loss: F(1,40) = 0.240, p = .627, $\eta^2 = .001$ Group by time interaction in responses to loss: F(12, 480) = 1.339, p = .193, $\eta^2 = .028$

Right pre-SMA signal change following gain and loss



Main effect of group in responses to gain: F(1,40) = 4.388, p = .043, $\eta^2 = 0.013*$ Group by time interaction in responses to gain: F(4.36, 174.23) = 0.637, p = .650, $\eta^2 = 0.014$ Main effect of group in responses to loss: F(1,40) = 0.030, p = .864, $\eta^2 < .001$ Group by time interaction in responses to loss: F(4.69, 187.54) = 1.325, p = .257, $\eta^2 = .027$

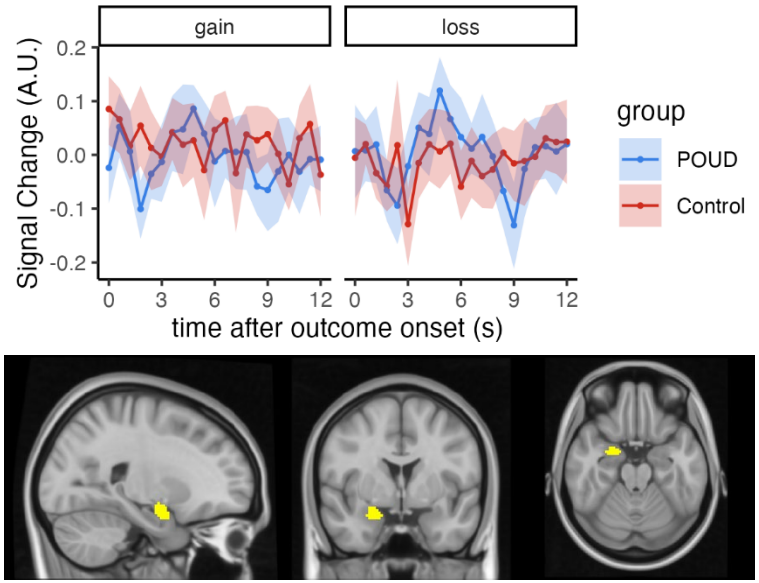
Left amygdala signal change following gain and loss



Main effect of group in responses to gain: F(1,40) = 0.383, p = .539, $\eta^2 = 0.001$ Group by time interaction in responses to gain: F(12, 480) = 1.415, p = .155, $\eta^2 = 0.034$ Main effect of group in responses to loss: F(1,40) = 0.580, p = .451, $\eta^2 = 0.001$

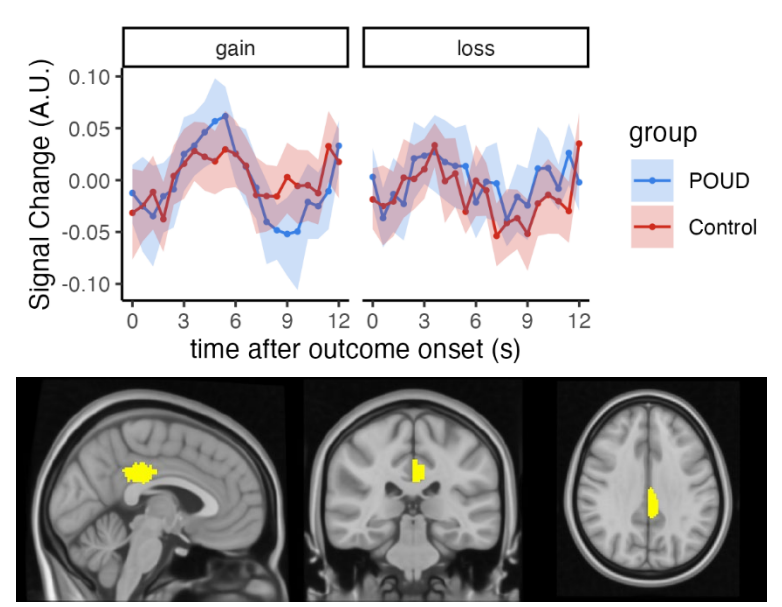
Group by time interaction in responses to loss: F(7.74, 309.7) = 1.497, p = .160, $\eta^2 = 0.034$

Right amygdala signal change following gain and loss



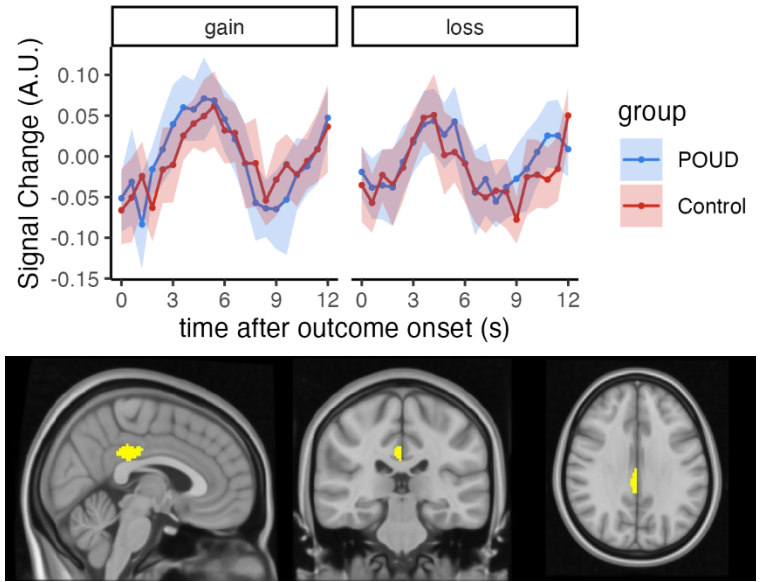
Main effect of group in responses to gain: F(1,40) = 2.582, p = .116, $\eta^2 = 0.001$ Group by time interaction in responses to gain: F(12, 480) = 1.588, p = .091, $\eta^2 = 0.034$ Main effect of group in responses to loss: F(1,40) = 6.451, p = .015, $\eta^2 = 0.010*$ Group by time interaction in responses to loss: F(7.38, 295.24) = 1.375, p = .212, $\eta^2 = 0.031$

Left posterior cingulate signal change following gain and loss



Main effect of group in responses to gain: F(1,40) = 1.368, p = .249, $\eta^2 = 0.004$ Group by time interaction in responses to gain: F(6.41, 256.32) = 0.454, p = .853, $\eta^2 = 0.001$

Main effect of group in responses to loss: F(1,40) = 0.398, p = .532, $\eta^2 = 0.001$ Group by time interaction in responses to loss: F(6.25, 250.06) = 0.738, p = .625, $\eta^2 = 0.016$ Right posterior cingulate signal change following gain and loss



Main effect of group in responses to gain: F(1,40) = 1.705, p = .199, $\eta^2 = 0.005$ Group by time interaction in responses to gain: F(6.69, 267.52) = 0.628, p = .725, $\eta^2 = 0.013$ Main effect of group in responses to loss: F(1,40) = 0.046, p = .832, $\eta^2 < 0.001$ Group by time interaction in responses to loss: F(6.32, 252.67) = 0.370, p = .905, $\eta^2 = 0.008$

References

Abraham, Alexandre, Fabian Pedregosa, Michael Eickenberg, Philippe Gervais, Andreas Mueller, Jean Kossaifi, Alexandre Gramfort, Bertrand Thirion, and Gael Varoquaux. 2014. "Machine Learning for Neuroimaging with Scikit-Learn." Frontiers in Neuroinformatics 8. https://doi.org/10.3389/fninf.2014.00014.

Avants, B.B., C.L. Epstein, M. Grossman, and J.C. Gee. 2008. "Symmetric Diffeomorphic Image Registration with Cross-Correlation: Evaluating Automated Labeling of Elderly and Neurodegenerative Brain." Medical Image Analysis 12 (1): 26–41. https://doi.org/10.1016/j.media.2007.06.004.

Bartra, O., McGuire, J. T., & Kable, J. W. (2013). The valuation system: A coordinate-based metaanalysis of BOLD fMRI experiments examining neural correlates of subjective value. *NeuroImage*, 76, 412–427.

Behzadi, Yashar, Khaled Restom, Joy Liau, and Thomas T. Liu. 2007. "A Component Based Noise Correction Method (CompCor) for BOLD and Perfusion Based fMRI." NeuroImage 37 (1): 90–101. https://doi.org/10.1016/j.neuroimage.2007.04.042.

Cox, Robert W., and James S. Hyde. 1997. "Software Tools for Analysis and Visualization of fMRI Data." NMR in Biomedicine 10 (4-5): 171–78. https://doi.org/10.1002/(SICI)1099-1492(199706/08)10:4/5<171::AID-NBM453>3.0.CO;2-L

Esteban, Oscar, Ross Blair, Christopher J. Markiewicz, Shoshana L. Berleant, Craig Moodie, Feilong Ma, Ayse Ilkay Isik, et al. 2018. "FMRIPrep." Software. Zenodo. https://doi.org/10.5281/zenodo.852659.

Esteban, Oscar, Christopher Markiewicz, Ross W Blair, Craig Moodie, Ayse Ilkay Isik, Asier Erramuzpe Aliaga, James Kent, et al. 2018. "fMRIPrep: A Robust Preprocessing Pipeline for Functional MRI." Nature Methods. https://doi.org/10.1038/s41592-018-0235-4.

Evans, AC, AL Janke, DL Collins, and S Baillet. 2012. "Brain Templates and Atlases." NeuroImage 62 (2): 911–22. https://doi.org/10.1016/j.neuroimage.2012.01.024.

Glasser, Matthew F., Stamatios N. Sotiropoulos, J. Anthony Wilson, Timothy S. Coalson, Bruce Fischl, Jesper L. Andersson, Junqian Xu, et al. 2013. "The Minimal Preprocessing Pipelines for the Human Connectome Project." NeuroImage, Mapping the connectome, 80: 105–24. https://doi.org/10.1016/j.neuroimage.2013.04.127.

Gorgolewski, K., C. D. Burns, C. Madison, D. Clark, Y. O. Halchenko, M. L. Waskom, and S. Ghosh. 2011. "Nipype: A Flexible, Lightweight and Extensible Neuroimaging Data Processing Framework in Python." Frontiers in Neuroinformatics 5: 13. https://doi.org/10.3389/fninf.2011.00013.

Gorgolewski, Krzysztof J., Oscar Esteban, Christopher J. Markiewicz, Erik Ziegler, David Gage Ellis, Michael Philipp Notter, Dorota Jarecka, et al. 2018. "Nipype." Software. Zenodo. https://doi.org/10.5281/zenodo.596855.

Greve, Douglas N, and Bruce Fischl. 2009. "Accurate and Robust Brain Image Alignment Using Boundary-Based Registration." NeuroImage 48 (1): 63–72. https://doi.org/10.1016/j.neuroimage.2009.06.060.

Jenkinson, Mark, Peter Bannister, Michael Brady, and Stephen Smith. 2002. "Improved Optimization for the Robust and Accurate Linear Registration and Motion Correction of Brain Images." NeuroImage 17 (2): 825–41. https://doi.org/10.1006/nimg.2002.1132.

Jenkinson, Mark, and Stephen Smith. 2001. "A Global Optimisation Method for Robust Affine Registration of Brain Images." Medical Image Analysis 5 (2): 143–56. https://doi.org/10.1016/S1361-8415(01)00036-6.

Lanczos, C. 1964. "Evaluation of Noisy Data." Journal of the Society for Industrial and Applied Mathematics Series B Numerical Analysis 1 (1): 76–85. https://doi.org/10.1137/0701007.

Power, Jonathan D., Anish Mitra, Timothy O. Laumann, Abraham Z. Snyder, Bradley L. Schlaggar, and Steven E. Petersen. 2014. "Methods to Detect, Characterize, and Remove Motion Artifact in Resting State fMRI." NeuroImage 84 (Supplement C): 320–41. https://doi.org/10.1016/j.neuroimage.2013.08.048.

Pruim, Raimon H. R., Maarten Mennes, Daan van Rooij, Alberto Llera, Jan K. Buitelaar, and Christian F. Beckmann. 2015. "ICA-AROMA: A Robust ICA-Based Strategy for Removing Motion Artifacts from fMRI Data." NeuroImage 112 (Supplement C): 267–77. https://doi.org/10.1016/j.neuroimage.2015.02.064.

Satterthwaite, Theodore D., Mark A. Elliott, Raphael T. Gerraty, Kosha Ruparel, James Loughead, Monica E. Calkins, Simon B. Eickhoff, et al. 2013. "An improved framework for confound regression and filtering for control of motion artifact in the preprocessing of resting-state functional connectivity data." NeuroImage 64 (1): 240–56. https://doi.org/10.1016/j.neuroimage.2012.08.052.

Tustison, N. J., B. B. Avants, P. A. Cook, Y. Zheng, A. Egan, P. A. Yushkevich, and J. C. Gee. 2010. "N4ITK: Improved N3 Bias Correction." IEEE Transactions on Medical Imaging 29 (6): 1310–20. https://doi.org/10.1109/TMI.2010.2046908.

Zhang, Y., M. Brady, and S. Smith. 2001. "Segmentation of Brain MR Images Through a Hidden Markov Random Field Model and the Expectation-Maximization Algorithm." IEEE Transactions on Medical Imaging 20 (1): 45–57. https://doi.org/10.1109/42.906424.